

# Quantitative trait locus mapping identifies a locus linked to striatal dopamine and points to collagen IV alpha-6 chain as a novel regulator of striatal axonal branching in mice

Mélanie H. Thomas<sup>1,2</sup> | Yujuan Gui<sup>3</sup> | Pierre Garcia<sup>1,2,4</sup> | Mona Karout<sup>1</sup> |  
 Borja Gomez Ramos<sup>1,3</sup> | Christian Jaeger<sup>1</sup> | Alessandro Michelucci<sup>1,5</sup> |  
 Anthoula Gaigneaux<sup>3</sup> | Heike Kollmus<sup>6</sup> | Arthur Centeno<sup>7</sup> | Klaus Schughart<sup>6,8,9</sup> |  
 Rudi Balling<sup>1</sup> | Michel Mittelbronn<sup>1,2,3,4,5</sup> | Joseph H. Nadeau<sup>10,11</sup> |  
 Thomas Sauter<sup>3</sup> | Robert W. Williams<sup>7</sup> | Lasse Sinkkonen<sup>3</sup> | Manuel Buttini<sup>1,2</sup>

<sup>1</sup>Luxembourg Centre for Systems Biomedicine (LCSB), University of Luxembourg, Esch/Alzette, Luxembourg

<sup>2</sup>Luxembourg Centre of Neuropathology (LCNP), Luxembourg

<sup>3</sup>Department of Life Sciences and Medicine (DLSM), University of Luxembourg, Belvaux, Luxembourg

<sup>4</sup>National Center of Pathology (NCP), Laboratoire National de Santé (LNS), Dudelange, Luxembourg

<sup>5</sup>Neuro-Immunology Group, Department of Oncology (DONC), Luxembourg Institute of Health (LIH), Luxembourg, Luxembourg

<sup>6</sup>Department of Infection Genetics, Helmholtz Centre for Infection Research, Braunschweig, Germany

<sup>7</sup>Department of Genetics, Genomics and Informatics, University of Tennessee Health Science Center, Memphis, Tennessee, USA

<sup>8</sup>University of Veterinary Medicine Hannover, Hannover, Germany

<sup>9</sup>Department of Microbiology, Immunology and Biochemistry, University of Tennessee Health Science Center, Memphis, Tennessee, USA

<sup>10</sup>Pacific Northwest Research Institute, Seattle, Washington, USA

<sup>11</sup>Maine Medical Center Research Institute, Scarborough, Maine, USA

## Correspondence

Lasse Sinkkonen, Department of Life Sciences and Medicine (DLSM), University of Luxembourg, Belvaux, Luxembourg.  
 Email: [lasse.sinkkonen@uni.lu](mailto:lasse.sinkkonen@uni.lu)

Manuel Buttini, Luxembourg Centre for Systems Biomedicine (LCSB), University of Luxembourg, Esch/Alzette, Luxembourg.  
 Email: [manuel.buttni@uni.lu](mailto:manuel.buttni@uni.lu)

## Funding information

Fonds National de la Recherche Luxembourg,  
 Grant/Award Numbers: FNR CORE  
 C15/BM/10406131, FNR PEARL  
 P16/BM/11192868; Helmholtz-Association  
 (Program Infection and Immunity)

## Abstract

Dopaminergic neurons (DA neurons) are controlled by multiple factors, many involved in neurological disease. Parkinson's disease motor symptoms are caused by the demise of nigral DA neurons, leading to loss of striatal dopamine (DA). Here, we measured DA concentration in the dorsal striatum of 32 members of Collaborative Cross (CC) family and their eight founder strains. Striatal DA varied greatly in founders, and differences were highly heritable in the inbred CC progeny. We identified a locus, containing 164 genes, linked to DA concentration in the dorsal striatum on chromosome X. We used RNAseq profiling of the ventral midbrain of two founders with substantial difference in striatal DA—C56BL/6 J and A/J—to highlight potential protein-coding candidates modulating this trait. Among the five differentially expressed genes within the locus, we found that the gene coding for the collagen IV

Mélanie H. Thomas and Yujuan Gui contributed equally to this work

This is an open access article under the terms of the Creative Commons Attribution-NonCommercial-NoDerivs License, which permits use and distribution in any medium, provided the original work is properly cited, the use is non-commercial and no modifications or adaptations are made.

© 2021 The Authors. Genes, Brain and Behavior published by International Behavioural and Neural Genetics Society and John Wiley & Sons Ltd.

alpha 6 chain (*Col4a6*) was expressed nine times less in A/J than in C57BL/6J. Using single cell RNA-seq data from developing human midbrain, we found that *COL4A6* is highly expressed in radial glia-like cells and neuronal progenitors, indicating a role in neuronal development. Collagen IV alpha-6 chain (*COL4A6*) controls axogenesis in simple model organisms. Consistent with these findings, A/J mice had less striatal axonal branching than C57BL/6J mice. We tentatively conclude that DA concentration and axonal branching in dorsal striatum are modulated by *COL4A6*, possibly during development. Our study shows that genetic mapping based on an easily measured Central Nervous System (CNS) trait, using the CC population, combined with follow-up observations, can parse heritability of such a trait, and nominate novel functions for commonly expressed proteins.

#### KEY WORDS

collaborative cross, dopamine, nigrostriatal circuit, Parkinson's disease, QTL, regulatory variants, tyrosine hydroxylase

## 1 | INTRODUCTION

Dopamine (DA) is one of the main neurotransmitters in the mammalian brain. It regulates several brain activities, such as motor and cognitive functions. Two important populations of DA neurons, with distinct functions, are located in the substantia nigra (SN) and ventral tegmental area (VTA) in the ventral midbrain, respectively. The DA neurons in the SN project mainly to the dorsal striatum, controlling motor function, while the ones in the VTA project mainly to nucleus accumbens and amygdala, controlling reward and emotion, or to the cortex and hippocampus, modulating cognition and memory.<sup>1,2</sup> Both DA neuron populations are at the center of research because of their involvement in neurological diseases, notably VTA DA neurons in neuropsychiatric disorders, and SN DA neurons in Parkinson's disease (PD).

Because of its prevalence and costs to society, PD has received much attention. Environmental and genetic risk factors contribute to the variability of PD features.<sup>3–6</sup> Age of onset, severity, rate of progression of PD motor symptoms, as well as the response to DA replacement therapies, vary greatly and are likely because of polymorphism in genes of the nigrostriatal circuit.<sup>7,8</sup> Genetic factors governing the development of this circuit and its baseline functions in adults are frequently those that are dysregulated in PD.<sup>9</sup> Hence, a better understanding of genetic variation associated with these factors could pave the way for a better understanding of PD.

As studies with standardized environments are difficult in humans, mouse models are used to study genetic variations. The mouse shares similar brain architecture and 99% of genes with humans, and allows for cost-effective and controlled studies.<sup>10</sup> Phenotypic differences in the dopaminergic circuit and related behaviors in rodents are based on genetic variation. Differences in DA neuron cell number and striatal DA level have been reported between different strains of mice.<sup>11–15</sup> Motor behavior and susceptibility to PD

toxins differ between strains.<sup>16–19</sup> Recombinant inbred mouse strains are commonly used to identify candidate genes by QTL mapping.<sup>20</sup> Collaborative Cross (CC) strains are a collection of such strains and are derived from eight founder strains.<sup>21</sup>

In this study, we used CC strains to map a QTL linked to DA level in the dorsal striatum. We measured DA concentration in the dorsal striata of eight CC founders and 32 derived CC strains, and observed that this trait was dictated in large part by the genetic background of the strains. We identified a QTL associated with striatal DA concentration on chromosome X that contained 164 genes. This showed that the CNS trait of striatal DA is inheritable. As a first step toward identification of expressed gene candidates modulating this trait, we analyzed previously generated transcriptome data of the ventral midbrains of C57BL/6J and A/J mice, two CC founders with large striatal DA differences. Within the QTL region, five differentially expressed genes were identified, with *Col4a6* showing 9-fold lower expression in A/J than in C57BL/6J mice. Single cell RNA-seq data of developing human midbrain have showed that *COL4A6* expression is modulated during development, indicating a role in neurogenesis.<sup>22</sup> Studies in simple models (*Drosophila*, zebra fish) support a role of the *Col4a6* gene product in axon guidance and outgrowth during brain development.<sup>23,24</sup> Interestingly, our measurements of tyrosine-hydroxylase (TH, a key enzyme in DA biosynthesis)-positive axons in projection areas of SN DA neurons (dorsal striatum) and of VTA DA neurons (piriform cortex, basolateral amygdala) showed that axonal branching of SN DA neurons, but not that of VTA DA neurons, is less dense in A/J than in C57BL/6J mice. However, the area occupied by TH-positive neuronal profiles in the SN did not differ between these two strains, indicating that a difference in the number of nigral TH-neurons between the two strains was not the cause of the observed difference in striatal branching. Our observations show that DA concentration in the dorsal striatum is inheritable, and indicate that differences of *Col4a6* expression during development could lead to differences in DA striatal innervation.

## 2 | MATERIALS AND METHODS

### 2.1 | Animals

Eight CC founder strains (A/J, C57BL/6J, 129S1Sv/ImJ, CAST/EiJ, PWK/PhJ, WSB/EiJ, NOD/ShiLtJ and NZO/HILtJ), were originally obtained from Jackson laboratories (Bar Harbor, Maine), and 32 CC strains (supplemental Table 1) were originally obtained from the University of North Carolina, Chapel Hill (UNC). Mice were bred at Chapel Hill or at the Central Animal Facilities of the Helmholtz Centre for Infection Research (Braunschweig, Germany). Animals were group housed. Animals that had been bred up at Jackson laboratories or at Chapel Hill, and transported to Braunschweig for work-up (without further breeding), were allowed to acclimatize for at least 2 weeks before euthanasia and extraction of brains. All mice were 3-month-old at the time of euthanasia. Ten to 12 mice per strain (mixed males and females) were anesthetized with a ketamine-medetomidine mix (150 and 1 mg/kg, respectively). Intracardial perfusion with PBS was performed to remove the blood. The brains were extracted from the skulls and halved along the midline with a razor blade. One hemibrain (brain hemisphere) was placed on a cooled metal plate over ice and regions of interest were dissected out with Dumont forceps. The dorsal striatum and ventral midbrain were identified using anatomical landmarks. These regions were identified visually on the cut medial surface of the hemibrain. The dorsal striatum was collected by carefully removing cortical tissue and brain tissue caudal of the fimbria and dorsal of the ventral commissure. The ventral midbrain was removed as described.<sup>25,26</sup> Briefly, the hemibrain was placed ventral side up on a metal plate over ice, and the region of interest that was removed was caudally of the hypothalamus and thalamus, rostrally of the pons, and ventrally of the medial lemniscus, and inferior colliculus. The second hemibrain was fixed in paraformaldehyde (PFA) 4% for 48 h, and then transferred to PBS with 0.5% sodium azide as preservative, until further processing for histology.

The experiments were performed according to the national guidelines of the animal welfare law in Germany (BGBl. I S. 1206, 1313 and BGBl. I S. 1934) and the European Communities Council Directive 2010/63/EU. The protocol was reviewed and approved by the “Niedersächsisches Landesamt für Verbraucherschutz und Lebensmittelsicherheit, Oldenburg, Germany” (Permit Numbers: 33.9-42,502-05-11A193, 33.19-42,502-05-19A394), respecting the 3Rs' requirements for Animal Welfare.

### 2.2 | DA measurement by gas chromatography-mass spectrometry

Striatal DA levels were measured in CC founders and 32 CC strains. The tissue homogenization and metabolite extraction were performed at 4°C to prevent changes in the metabolic profile. As this study progressed over a couple of years, the method for DA measurement was optimized, and hence, DA in the first set of CC founders were measured by a different, less straightforward method than in a second set

of CC founders and all 32 CC strains. To not use additional mice to repeat the initial measurements (in accordance with E.U.'s 3R's guidelines for animal use), we present here the results for all CC founders as percentage of the mean of C57BL/6J, a reference strain in the neurosciences.<sup>27</sup>

The first method was described previously.<sup>28</sup> The dorsal striatum of each mouse was pulverized in a bead mill with metal grinding beads (7 mm). The samples were then homogenized in the bead mill with smaller grinding beads (1 mm) and the extraction fluid (methanol/distilled water, 40:8.5 vol/vol). The metabolites were extracted using a liquid–liquid extraction method first by addition of chloroform to the tissue fluid followed by distilled water. After shaking for 20 min at 1300 rpm at 4°C, the mixture was centrifuged for 5 min at 5000 × g at 4°C. The upper phase containing the polar metabolites was transferred to a sample vial for speed vacuum evaporation. The second method was also described previously.<sup>29</sup> The difference to method 1 is that ceramic beads are used instead of metal ones, and it was slightly modified to reduce the runtime.<sup>29</sup>

For both methods, the resulting dried samples were derivatized using an established procedure. Twenty microliter of pyridine (containing 20 mg/ml of methoxyamine hydrochloride) were added to the samples and incubated at 45°C with continuous shaking for 90 min. Then 20 µl of MSTFA were added to the sample vial and incubated 30 min at 45°C with continuous shaking.

After derivatization, the gas chromatography-mass spectrometry (GC-MS) analysis was performed with an Agilent 7890A GC, or 7890B for the second method, coupled to an Agilent 5975C inert XL mass selective detector (MSD) or 5977A for the second method (Diegem, Belgium). One microliter of sample was injected into a Split/Splitless inlet operating in split mode (10:1) at 270°C. Helium was used as a carrier gas with a constant flow rate of 1.2 ml/min. The transfer line temperature was set constantly to 280°C and the MSD was operating under electron ionization at 70 eV. As described by Jäger et al.,<sup>29</sup> a multi-analyte detection using a quadrupole analyzer in selected ion monitoring mode was used for a sensitive and precise quantification of DA and the internal standard DA-d4.

### 2.3 | Quantitative immunofluorescence of tyrosine-hydroxylase positive neuronal components

TH protein was measured by quantitative immunofluorescence in the dorsal striatum, basolateral amygdala, piriform cortex and SN of 3-month-old C57BL/6J and A/J mice. After fixation in phosphate-buffered 4% paraformaldehyde for 48 h, hemibrains were stored in PBS with 0.2% of sodium azide at 4°C until work-up. Parasagittal free-floating sections (50 µm) were generated using a vibratome (Leica; VT 1000S). Sections were collected sequentially in a set of eight tubes/mouse, containing a cryoprotective medium (polyvinyl pyrrolidone 1% wt/vol in PBS/ethylene glycol 1:1), then stored at –20°C until use. The lateral sections were collected for the dorsal striatum, basolateral amygdala and piriform cortex measurements and the medial sections were collected for the SN measurements.

The sections were washed in PBS with 0.1% Triton X-100 (PBST) and permeabilized in PBS with 3% H<sub>2</sub>O<sub>2</sub> and 1.5% Triton X-100. The sections were then blocked for 1 h in PBST with 5% bovine serum albumin (BSA), and incubated overnight with rabbit anti-TH antibody (1:1000, Millipore, AB152) diluted in the same buffer. After three washing steps in PBS, the sections were incubated for 2 h with the secondary antibody (Alexa fluor 488 goat anti-rabbit 1:1000, Invitrogen), then mounted on slides and embedded in fluoromount-G (Southern Biotech).

Imaging was performed using a Zeiss AxioImager Z1 upright microscope, coupled to a “Colibri” LED system, and an Mrm3 digital camera for image capture using the software Zeiss Zen 2 Blue. For each striatum, basolateral amygdala and piriform cortex on each section, 2–3 images/section (out of a total of three randomly selected sections per animal) were taken at  $\times 40$  magnification using the Zeiss Apotome<sup>R</sup> system. After thresholding, the area occupied by TH-positive stainings in each picture was determined using the FIJI imaging software.<sup>30,31</sup> For the SN sections, the pictures were taken at  $\times 10$  magnification. The area occupied by TH-positive neuronal profiles was measured in the region of interest, the SN, using ImageJ FIJI software. We measured four different anatomical levels of the SN, from medial to lateral, covering the entire region of interest. Each area was quantified and averaged separately, and all were summed as a cumulated surface ( $\text{mm}^2$ ). Details on the validation of this approach, used as indirect measure for the number of TH-positive neurons, by stereological count estimates of TH-positive cells can be found in the supplemental material of Reference 32.

All measurements were performed on blinded sections, and codes were not broken until the analysis was complete. The difference in striatal TH in C57BL/6J versus A/J mice (see results) was confirmed by two independent investigators (Mélanie H. Thomas and Mona Karout) on independent sets of sections.

## 2.4 | Cell culture

Human small molecule neuroepithelial precursor cells (smNPCs) were differentiated from a previously established induced pluripotent stem (iPS) cell line from a healthy 67-year old male donor.<sup>33</sup> Differentiation of smNPCs toward ventral neural tube lineages, including DA neurons, was carried out for 30 days as previously described.<sup>34</sup>

## 2.5 | cDNA synthesis

Total RNA was extracted using Quick-RNA Miniprep Kit from Zymo Research (R1055) as per manufacturer instructions. cDNA synthesis was performed using 1  $\mu\text{g}$  of total RNA, 2.5  $\mu\text{M}$  oligo dT-primer, 0.5 mM dNTPs from ThermoFisher (R0181), 1  $\mu\text{l}$  Ribolock RNase inhibitor (40 U/ $\mu\text{l}$ ) from ThermoFisher (EO0381) and 1  $\mu\text{l}$  RevertAid Reverse Transcriptase (200 U/ $\mu\text{l}$ ) from ThermoFisher (EP0441). The final volume of the reaction mix was 40  $\mu\text{l}$ . The reaction was incubated at 42°C for 1 h. The reaction was terminated by incubating at 70°C for 10 min. The cDNA was diluted 1:10 in DNase/RNase free water, and stored at –20°C.

## 2.6 | Reverse-transcription quantitative Polymerase Chain Recation (RT-qPCR)

RT-qPCR was performed with the Applied Biosystems 7500 Fast Real-Time PCR System using 1xAbsolute Blue qPCR SYBR green low-ROX mix from ThermoFisher (AB4322B), 5  $\mu\text{l}$  of diluted cDNA and 500 nM primer concentration, in a final volume of 20  $\mu\text{l}$ . The conditions of the PCR reaction were 95°C for 15 min and repeating 40 cycles of 95°C for 15 s, 55°C for 15 s and 72°C for 30 s. The gene expression level was calculated using the  $2^{-(\Delta\Delta Ct)}$  method. The  $\Delta\Delta Ct$  refers to  $(\Delta Ct_{(\text{target gene})} - \Delta Ct_{(\text{housekeeping gene})})_{\text{Neurons}} - (\Delta Ct_{(\text{target gene})} - \Delta Ct_{(\text{housekeeping gene})})_{\text{smNPC}}$ . ACTB was used as the housekeeping gene. The following primer sequences were used: ACTB (forward), 5'-AAACTGGAACGGTG-3'; ACTB (reverse), 5'-AGAG AAGTGGGTGGCTTT-3'; SOX2 (forward), 5'-CCCTTTATTTCC GTAGTTGTATT-3'; SOX2 (reverse), 5'-GATTCTCGGCAGACTGATT CAA-3'; COL4A6 (forward), 5'-CTGGCTTCTGGCATCAAT-3'; COL4A6 (reverse), 5'-CTACCTGGAGCAAGGACAGG-3'.

## 2.7 | Quantitative trait locus mapping

The QTL mapping was performed using [www.genenetwork.org/](http://www.genenetwork.org/).<sup>35</sup> The dataset with DA measurements of dorsal striata of 32 CC strains can be located with search terms (Species: Mouse [mm10]; Group: CC Family; Type: Traits and Cofactors; Dataset: CC Phenotypes), then by navigating to Record CCF\_10,039. QTL mapping was performed with GEMMA on all chromosomes, MAF > = 0.05 with LOCO method. The genome wide significance of QTL mapping was set by 500 permutation simulations, with FDR under 5% for each scan.

GeneNetwork uses the GEMMA linear mixed model to map complex populations, and has been used to map loci in interbreds,<sup>36</sup> advanced intercross lines,<sup>37,38</sup> and outbreds.<sup>39</sup> GEMMA accounts for kinship relations among cases and strains. The GEMMA algorithm used here is described elsewhere,<sup>40</sup> and its use in the context of GeneNetwork has recently been described.<sup>41</sup>

## 2.8 | Estimation of striatal DA level heritability in CC strains

The heritability ( $h^2$ ) was estimated as described.<sup>42</sup> Briefly, the total phenotypic variance ( $V_p$ ) is calculated on all CC strains. The additive genetic variance ( $V_a$ ) was estimated by the mean of within-strain variance. The heritability ( $h^2$ ) was calculated as  $V_a/V_p$ .

## 2.9 | Statistical analysis

Statistics were carried out with R (version 4.0.2), or PRISM v. 9 (Graphpad). Normality of the data was confirmed with Shapiro-Wilk test or Kolmogorov-Smirnov test. For the striatal DA concentration of founders, because we applied two different methods for measurement (see above), we used the mean of reference strain C57BL/6J<sup>27</sup> in each

method, and normalized all individual measurements from CC founders to that value. After confirming that the normalized data was still normally distributed and that the standard deviation of the normalized data did not differ substantially (over 10%) for those of the original data sets, the data from both measurement sets were combined. Two-way ANOVA was applied to the DA values of the eight founder strains, with strain, sex and strain-sex interaction taking into consideration. The resulting data was analyzed by three post-hoc tests: Tukey, Two-stage procedure of Benjamini, Krieger & Yekutieli, and, finally, Dunnett's using C57BL/6J as reference strain. All *p*-values were FDR corrected. For the striatal DA concentrations in CC strains, because we used only one method for DA measurement, we applied ANOVA directly on raw values, followed by Tukey, and two-stage procedure of Benjamini, Krieger & Yekutieli. The statistical analysis of RT-PCR data was performed with unpaired two-tailed *t*-test. The input value was delta Ct (*Actb* as the housekeeping gene). The statistical analysis for RNA-seq was performed in R with package DESeq2 (version: 1.28.1), details can be found in Reference 25. Two-tailed, unpaired-test was used to analyze the effect of strain (C57BL/6J vs. A/J) on TH-immunopositive neuronal structures in each brain region.

### 3 | RESULTS

#### 3.1 | Differences in striatal DA levels across CC mice are genetically controlled

Several phenotypic differences have been described between CC founders as well as CC mouse strains.<sup>43–45</sup> In this study, we started

by measuring DA concentration in dorsal striata from the eight inbred founder CC strains (Supplemental Table 2). Striatal DA is a key neurotransmitter regulating voluntary motor behavior.<sup>46</sup> In total, striatal DA level from 102 mice was measured by GC-MS. DA concentrations varied significantly across the founders (two-way ANOVA, *p*-value = 5.152e-05, *F* = 5.3212), showing strain-specific differences (Figure 1, supplemental Table 2). There was no difference between males and females (two-way ANOVA, sex *p*-value = 0.8626, *F* = 0.0301; strain:sex *p*-value = 0.8564, *F* = 0.4659), thus values for both sexes were pooled for each strain. *p* values from all pair-wise multiple comparisons are listed in supplemental Table 3. Because C57BL/6J is a reference strain in biomedicine,<sup>27</sup> in particular in neuroscience,<sup>47,48</sup> we used this strain to compare the striatal DA concentrations of the other seven founder strains to (Figure 1). PWK/PhJ, A/J and NOD/ShiLtJ strains showed the lowest concentrations of striatal DA, while the highest levels were detected in NZO/HILtJ, CAST/EiJ and C57BL/6J mice (supplemental Table 3 for *p* values of post-hoc tests). This result indicated that striatal DA is controlled genetically in mice.

To investigate if variation in striatal DA concentration is inheritable, we measured this trait in 32 CC mouse strains (Figure 2, supplemental Table 4). In total, we analyzed 327 CC mice with similar number of mice from both sexes in each strain. The CC strains showed considerable variation in striatal DA concentration, with a range of around 10 pmol/mg (Figure 2, two-way ANOVA, *p*-value <2e-16, *F* = 9.5587). There was no significant difference between males and females (two-way ANOVA, sex *p*-value = 0.5657, *F* = 0.3308; strain:sex *p* = 0.1343, *F* = 1.3093), thus the DA values

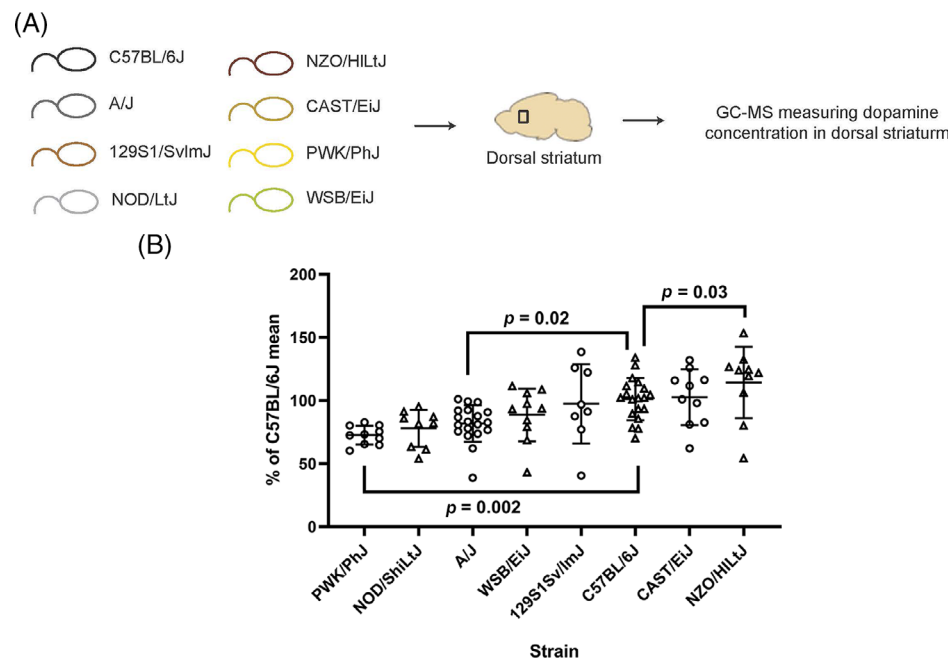


**FIGURE 1** Striatal dopamine (DA) concentration of eight Collaborative Cross (CC) founder strains. (A) Schematic representation of the experimental set-up. (B) DA concentration was measured by GC-MS in the dissected dorsal striata of one hemibrain/mouse of the eight CC founders. Because two different methods were used for DA measurements (see Section 2 for the reason), raw data in each of the two data sets were normalized to the mean of reference strain C57BL/6J, then combined. Data are means  $\pm$  SD. The significance of differences was tested by two-way ANOVA, considering strain (*p* = 5.152e-05, *F* value = 5.3212), sex (*p* = 0.8626, *F* value = 0.0301) and strain:sex interaction (*p* = 0.8564, *F* value = 0.4659). The post-hoc analysis was performed with Dunnett's post-hoc analysis, using the data of C57BL/6J strain as reference. Three strains (A/J, PWK/PhJ, and NZO/HILtJ) differ significantly from C57BL/6J. GC-MS, gas chromatography–mass spectrometry

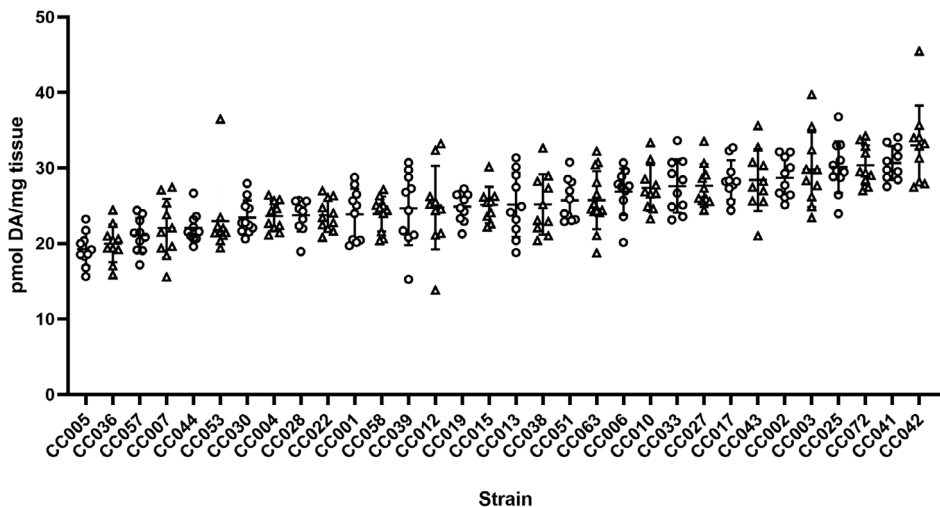


**FIGURE 2** Dorsal striatum dopamine (DA) concentration in 32 Collaborative Cross (CC) strains. DA concentration was measured by GC-MS in dorsal striata dissected from one hemibrain for each mouse. Data, expressed in pg/mg of tissue, are means  $\pm$  SD. Significance of differences was tested by two-way ANOVA considering strain ( $p < 2e-16$ , F value = 9.5587), sex ( $p = 0.5657$ , F value = 0.3308) and strain:sex interaction ( $p = 0.1343$ , F value = 1.3093). GC-MS, gas chromatography-mass spectrometry

for both sexes were grouped for each strain.  $P$  values from pair-wise multiple comparison tests are listed in supplemental Table 5.

The estimated heritability of striatal DA in CC strains ( $h^2$ ) was 0.52, indicating that striatal DA differences are inheritable (see Section 2 for details). In comparison, the heritability of the trait in founder strains was 0.31. The lower heritability in founder compared to CC strains is likely caused by the high variability of this trait in some founders strains, notably 129S1SvImJ, NZO/HILtJ and CAST/EiJ. Our results show that striatal DA is controlled genetically in mice, thus indicating that QTL mapping can be used to identify candidate genes associated with this trait.<sup>42,49</sup>

### 3.2 | QTL mapping associates a genomic locus on chromosome X with striatal DA levels

Identifying novel genetic regulators associated with striatal DA concentration could help better understand the development of DA circuits and susceptibility to diseases, such as PD. Therefore, to leverage the power of CC strains in identifying trait-associated genetic loci at a good resolution, we performed QTL mapping based on striatal DA concentration in 32 CC strains. The genome-wide significance of results for the top genetic markers is shown in Figure 3, and the full list is in supplemental Table 6. QTL mapping identified one genetic marker (SNP UNC31420222; rs29282811) located on chromosome X at position 144.300241 Mb ( $-\log_{10} p\text{-value} = 4.42$ , mm10 assembly) that is associated with striatal DA concentration. This linkage statistic was significant at the 0.05 genome-wide threshold of 4.38 (Figure 3). The 1.5 LOD support interval for the QTL extended from 139 Mb to 149 Mb, showing that this region harbors gene(s) that modulate striatal DA level.

### 3.3 | *Col4a6* is a developmental gene with altered expression between two founder mouse strains

QTL mapping can be a stepping-stone toward identification of candidate gene products that modulate biological traits associated with the

mapped locus. To determine if such a gene product candidates could be found in our study, we looked back at striatal DA data of the founder strains.

The C57BL/6J reference strain was one the founder strains with the highest striatal DA (Figure 1). Across CC strains, mice with the C57BL/6J genotype at marker rs2928281 had a mean striatal DA concentration of 28.162 pmol/mg, whereas mice that did have that C57BL/6J genotype had a mean striatal DA concentration of 24.111 pmol/mg. Because rs29282811 is located on the X chromosome, we assume that just one C57BL/6J allele was driving the higher average striatal DA in strains with that genotype.

Two CC founder strain mice, A/J and PWK/PhJ, had significantly lower striatal DA than C57BL/6J mice (Figure 1, supplemental Table 3), and a different genotype at rs29282811 ([https://www.sanger.ac.uk/sanger/Mouse\\_SnpViewer](https://www.sanger.ac.uk/sanger/Mouse_SnpViewer)). Interestingly, these mice have also been reported to perform less well in motor tests than C57BL/6J mice.<sup>50</sup> However, compared to C57BL/6J mice, A/J mice performed worse than PWK/PhJ mice in tests commonly used to test voluntary motor performance: open field (distance traveled and rearing events) and rotarod (Figure 3 in Reference 50). The lesser motor performance of A/J compared to C57BL/6J mice was already reported in an earlier study,<sup>18</sup> indicating that the difference between these two common laboratory strains is stable over generations and across labs. Thus, by looking more closely at the nigro-striatal circuit of C57BL/6J versus that of A/J mice, we set out to find new potential modulators of properties of that circuit.

The 10 Mb QTL from position 139 Mb to 149 Mb on chromosome X includes 164 genes that could potentially be associated with striatal DA concentration. The vast majority (>95%) of trait-associated genetic variants are located outside of protein-coding regions.<sup>51</sup> Therefore, we assumed that such regulatory variants could affect gene expression at our locus of interest in the ventral midbrain of C57BL/6J versus A/J mice. We first took advantage of our recent transcriptomic profiling of ventral midbrains from C57BL/6J and A/J mice.<sup>25</sup> Using their ventral midbrain RNA-seq data, we plotted the absolute log<sub>2</sub>-fold change for all 164 genes between C57BL/6J and

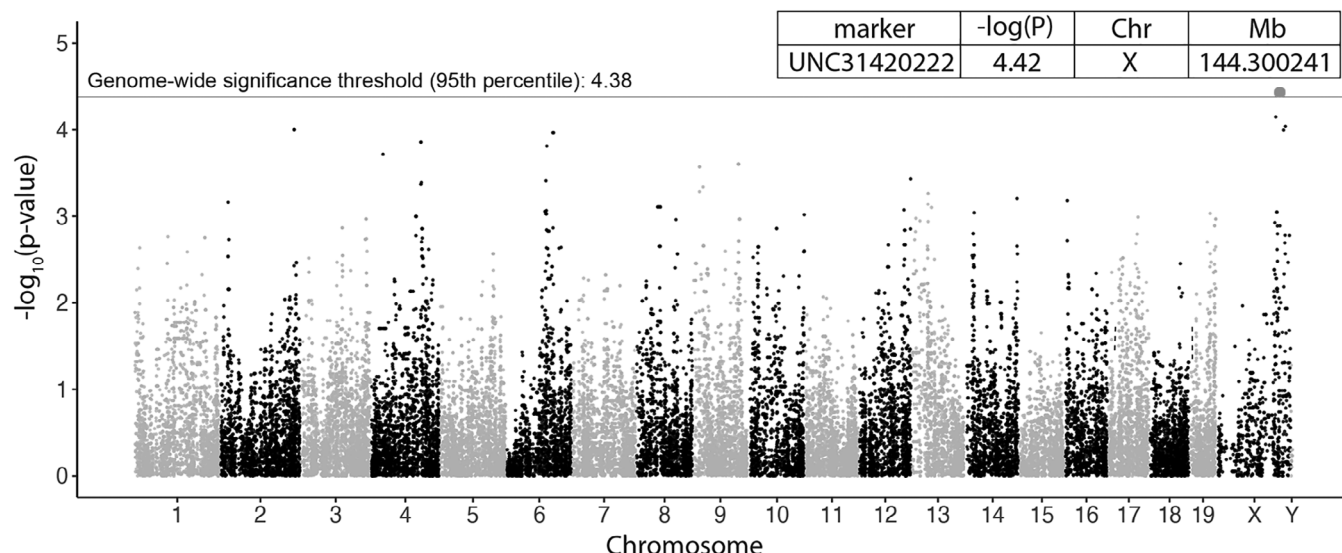


**FIGURE 3** QTL mapping for dorsal striatum dopamine concentration in CC strains. Plot shows  $-\log_{10} p$ -values (y-axis) of genetic markers across chromosome locations (x-axis). Horizontal dashed lines represent the 95th percentile thresholds for genome-wide significance  $-\log_{10} p$ -values = 4.38. QTL mapping with CC strains yielded the most significant QTL (in blue in the figure) at chromosome X 144.3 Mb with  $-\log_{10}(P)$  4.42. CC, Collaborative Cross

A/J in the QTL region to identify those with altered gene expression (Figure 4A). The transcriptomic analysis was based on a total of 24 mice, 12 from each strain (mixed sexes). Interestingly, only five genes showed significant differential gene expression (supplemental Table 7). By far the largest fold change of all protein-coding genes was found for the collagen IV subunit 6 (*Col4a6*) gene, which showed over 9-fold difference between the two strains, with A/J mice having significantly less *Col4a6* expression compared to C57BL/6J (Figure 4B,  $\log_{2}FC = -3.12$ ,  $p_{adj} = 6.28e^{-22}$ ). The differential expression of the four other DEGs between the two strains was quite low (Figure 4A, Supplemental Table 7). Moreover, the *Col4a6* transcription start site is located at position 141.474076 Mb, within the 10 Mb region of the QTL associated with striatal DA concentration, and approximately three centimorgan away from the rs29282811 marker.

While *Col4a6* expression was significantly lower in A/J than in C57BL/6J ventral midbrains, the overall level of expression in the adult C57BL/6J midbrain was also quite low (<0.3 RPKM), indicating its expression in adult mice is limited to only one or few cell types, most likely endothelial cells, which have been reported to produce collagens.<sup>52,53</sup> Collagen IV is an essential and abundant component of the basement membrane.<sup>54</sup> In the nervous system, its function has been associated with axon guidance and neurite outgrowth in simple model systems,<sup>23,24</sup> and in cultured neurons.<sup>55</sup>

To get a better idea about the cellular source of *COL4A6* during development, we performed RT-qPCR experiments with RNA collected from multipotent SOX2<sup>+</sup> human iPSC-derived neuroepithelial precursor cells, either in their undifferentiated state, or after 30 days of differentiation toward ventral neural tube lineages containing mainly neurons, including DA neurons.<sup>34</sup> Interestingly, *COL4A6* showed relatively high-expression levels in the neuronal progenitors and was strongly downregulated upon neuronal differentiation

(unpaired two-sided *t*-test, *p*-value = 4.468e-6), indicating that *COL4A6* is indeed developmentally regulated (Figure 4C). As expected, *COL4A6* reduction was accompanied by decreased SOX2 expression (unpaired two-sided *t*-test, *p*-value = 0.0003) during neuronal differentiation. To address the *in vivo* relevance of our findings on *COL4A6* level during development, we looked into its expression in published single cell RNA-seq (scRNA-seq) data corresponding to 26 cell types of the developing human midbrain.<sup>22</sup> *COL4A6* expression was highest in floor plate progenitors and selected subtypes of radial glia-like cells, but had very low expression detected in other cell types (Figure 4C). In keeping with our own results, the expression profile of *COL4A6* closely followed the expression of SOX2, a key regulator of neurogenesis.<sup>56</sup> Screens for primary SOX2 target genes have shown that *COL4A6* expression depends on SOX2,<sup>57,58</sup> supporting our observations.

Taken together, the expression profile of *COL4A6* implicates it is primarily a developmental gene and its dependence on SOX2 indicates a role in neurogenesis and axonal outgrowth.

### 3.4 | Differences in striatal axonal branching between C57BL/6J and A/J mice

Studies in zebra fish have shown that orthologs of type IV collagens, coded by gene products of *Col4a5* and *Col4a6*, control axonal guidance during development.<sup>24</sup> Based on the observed differences of A/J versus C57BL/6J mice in striatal DA concentration, motor performance,<sup>50</sup> the localization of *Col4a6* gene in the associated QTL, the distinct neurodevelopmental expression profile of *COL4A6*, and the role of collagen IV in neurite outgrowth and guidance (see references above), we hypothesized that DA neuron axonal fiber density

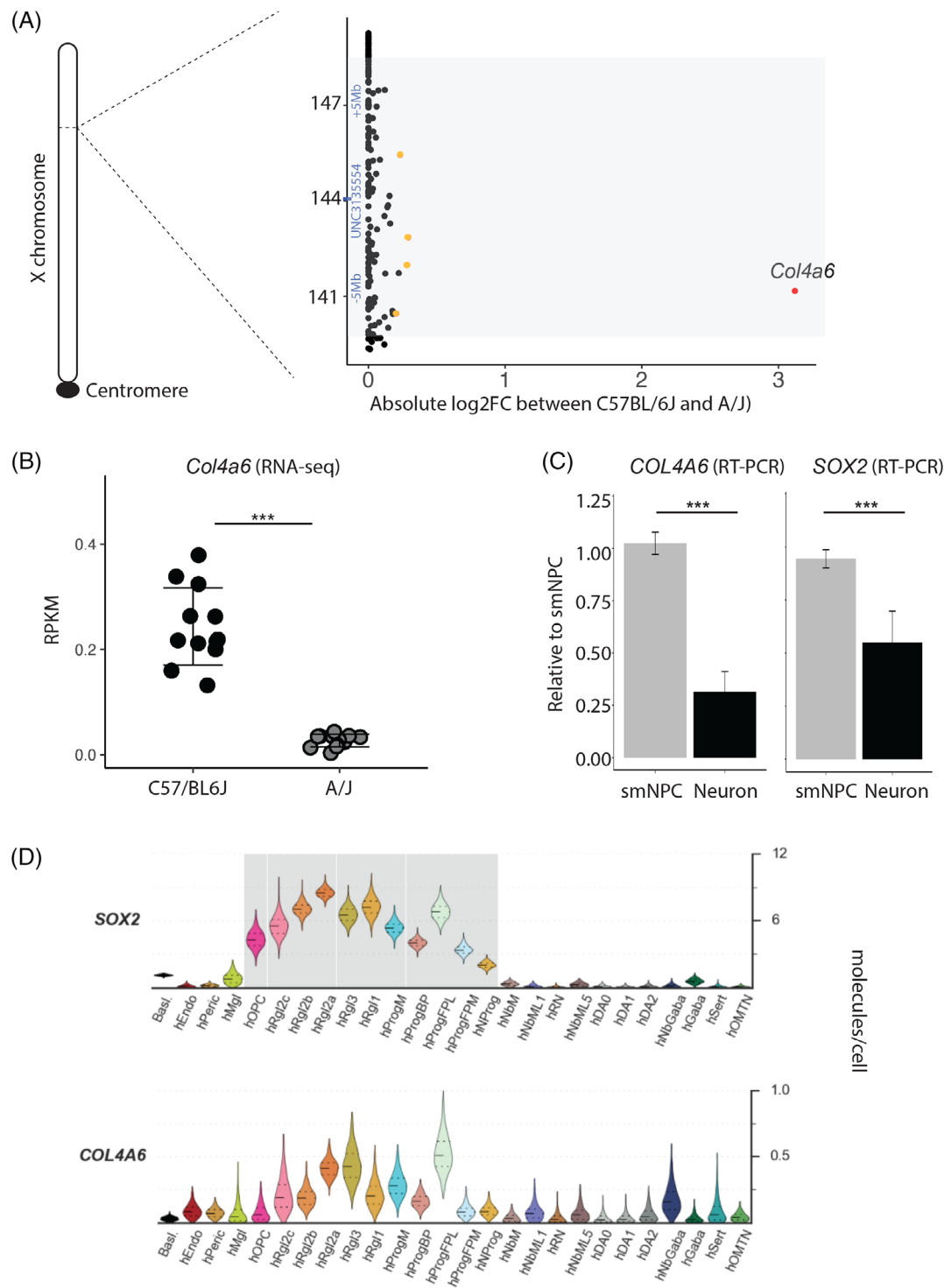


**FIGURE 4** *Col4a6*, a gene located in mapped QTL, shows high differential expression between C57BL/6J and A/J midbrains, and plays a role in neurogenesis. (A) Log<sub>2</sub>-fold changes of genes in chromosome X locus between 139 and 149 MB (highlighted with shade). Genes with adjusted *p*-value below 0.05 are labeled in orange for those with low-differential expression (list in Supplemental Table 7), and in red for *Col4a6*, the gene with the highest differential expression. (B) The expression (RPKM) of *Col4a6* in the ventral midbrain of C57BL/6J and A/J (*p*adj = 1.29e-22, \*\*\*). The data was derived from,<sup>25</sup> <https://doi.org/10.3389/fgene.2020.566734>. (C) RT-qPCR analysis of *COL4A6* and *SOX2* expression in undifferentiated *Sox2*<sup>+</sup> neuroepithelial precursor cells (smNPCs) and after 30 days of differentiation toward ventral neural tube lineages, including DA neurons. Significant downregulation of *COL4A6* (unpaired two-sided t-test, *p*-value = 4.468e-6, \*\*\*) and *SOX2* (unpaired two-sided t-test, *p*-value = 0.0003, \*\*\*) were observed upon neuronal differentiation. Measurements were carried out in triplicates. Bar show means ± SD. (D) The expression of *COL4A6* and *SOX2* during human midbrain development based on scRNA-seq data from La Manno et al.<sup>22</sup> The two genes show similar expression profiles. Cell types are named with “h” to indicate human: Endo, endothelial cells; Peric, pericytes; Mgl, microglia; OPC, oligodendrocyte precursor cells; Rgl1-3, radial glia-like cells; NProg, neuronal progenitor; Prog, progenitor medial floorplate (FPM), lateral floorplate (FPL), midline (M), basal plate (BP); NbM, medial neuroblast; NbML1&5, mediolateral neuroblasts; RN, red nucleus; DAO-2, dopaminergic neurons; Gaba, GABAergic neurons; Sert, serotonergic; OMTN, oculomotor and trochlear nucleus

would be different in the dorsal striatum of these two mouse strains. To test this, we performed TH immunostaining on brain sections from C57BL/6J and A/J mice (see Section 2). The percentage image area (in microphotographs) occupied by TH in the DA neuron projection areas (dorsal striatum for SN, piriform cortex and basolateral amygdala

for VTA) was used to compare axonal fiber density between the strains. Interestingly, A/J mice showed 29% lower TH-positive axonal density in the dorsal striatum compared to C57BL/6J mice (two-tailed unpaired t-test,  $p < 0.0001$ ,  $F = 2.1$ ) (Figure 5, Supplemental Table 8). No such differences were observed in the basolateral amygdala (two-

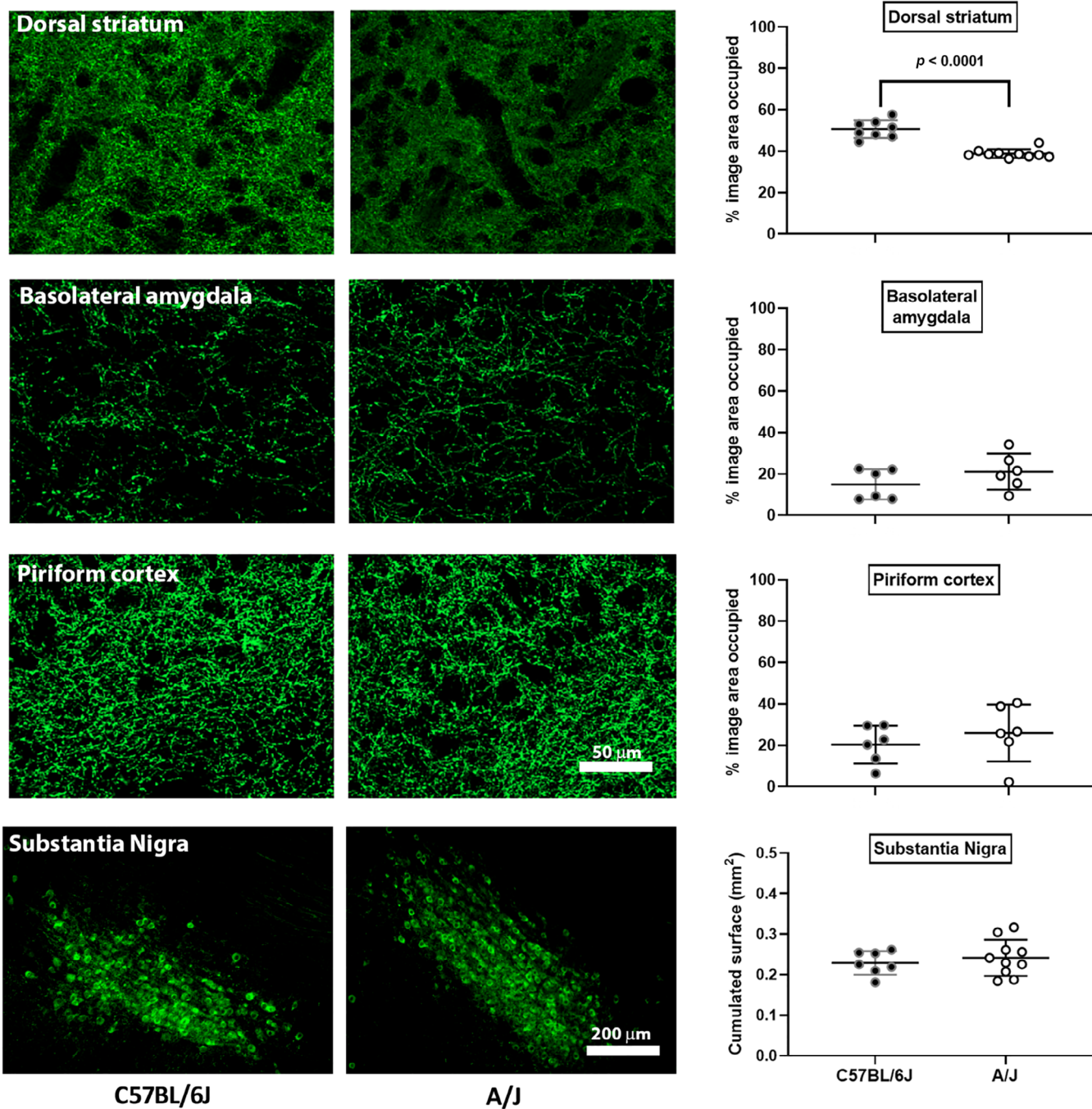


**FIGURE 5** Density of tyrosine hydroxylase (TH)-positive axons is higher in dorsal striatum of C57BL/6J mice than in that of A/J mice. Panels show TH-positive axons and their quantification in dorsal striatum (first row), basolateral amygdala (second row), piriform cortex (third row), and TH-positive neuronal profiles in Substantia Nigra (last row). Scale bar for all microphotographs of TH-positive axons is in second panel of third row (Piriform cortex in A/J; 50  $\mu$ m). Scale bar for microphotograph of TH-positive neuronal profiles is in second panel of last row (Substantia Nigra; 200  $\mu$ m). Scattergrams (3rd column) show quantification of the percentage image area occupied by TH-positive axons in striatum, basolateral amygdala, and piriform cortex, and of quantification of area occupied by the TH-positive neuronal profiles in Substantia Nigra (see main text for details). Data are expressed in mean  $\pm$  SD, and were analyzed with two-tailed, unpaired t-test

tailed unpaired *t*-test,  $p = 0.47$ ,  $F = 1.14$ ), or the piriform cortex (two-tailed unpaired *t*-test,  $p = 0.42$ ,  $F = 2.27$ ), suggesting that the differences observed between the two mouse strains was specific for the dorsal striatum.

We then looked at nigral DA neurons in C57BL/6J versus A/J mice. We used a morphometric approach that measured the area occupied by TH-positive neuronal profiles across the whole SN in the two strains, and that we have shown previously to correlate with stereological estimates of TH-positive neuronal counts (see Section 2, and supplemental material of Reference 32). We observed no difference in the area occupied by nigral TH-positive neuronal profiles between the two strains (two-tailed unpaired *t*-test,  $p = 0.78$ ,  $F = 1.29$ ), implying that differences observed in striatal TH positive axons in C57BL/6J versus A/J mice reflect a difference in branching of DA neurons, rather than their number in the SN (Figure 5, supplemental Table 8). Hence, our data points to a role of collagen IV alpha-6 chain (COL4A6) in modulating axonal branching of DA neurons of the SN, but not that of DA neurons of the VTA.

## 4 | DISCUSSION

While DA neurons residing in the SN are of central interest to translational neuroscience research because of their unique properties that renders them susceptible in PD,<sup>59</sup> many factors modulating their properties remain unknown. Uncovering factors that control their development, structure, and function help understand how they interrelate with other nervous system components in assuring the proper operations of the brain, or how they contribute to disease.<sup>9</sup>

In this study, we used CC strains to identify a locus and a candidate gene linked to properties of the DA neurons of the SN. The differences in striatal DA concentration between CC strains showed the considerable heritability of this trait. Together with previous transcriptomic data in the ventral midbrain of two founder strains, our results indicate that COL4A6 plays an important role in modulating axonal branching of nigral DA neurons. By increasing the number of CC strains, together with careful experimental study design,<sup>60</sup> more QTLs associated with this trait can probably be found, including some linked to markers that did not make it to significance in our study. Such follow-up studies could include mapping of loci linked to various additional neurochemical and neuroanatomical traits, at baseline or in response to disease, thus elevating the CC population to a key tool for translational neuroscience.

Despite the success of human GWAS methodologies to decipher phenotype–genotype associations, human tools lack proper standardized and controlled conditions. To overcome these limitations, CC mouse strains were generated to provide a model for heterogeneous human population.<sup>21,61,62</sup> Genetic diversity of CC mice provides more precise QTL mapping tool than conventional mapping populations. The wide phenotypic range of around 10 pmol/mg DA in the dorsal striatum enabled us to map a significant QTL of about 10 Mb with the reasonable number of 32 CC strains. To our knowledge, this is the first study mapping a QTL associated with a major mammalian CNS

neurotransmitter using the CC reference family. Our transcriptomic analysis of the ventral midbrain of 2 CC founders, C57BL/6J and A/J,<sup>25</sup> with significantly different concentration of striatal DA, helped us narrow down potential mediators driving striatal DA differences to five DEGs within this QTL. *Col4a6*, one of the DEGs, showed a 9-fold difference in expression between the two strains. To find out more about the role of *Col4a6* in the nigro-striatal brain circuit, we looked at data available from the developing human midbrain,<sup>22</sup> which suggested a role of COL4A6 in DA neuron neurogenesis. Collagen IV, alpha-6 chain, is one of the six subunits of type IV collagen, a major component of basement membranes. Collagen IV is a member of the collagen family of glycoproteins, which themselves are constituents of the extracellular matrix (ECM), and among the most abundant proteins in the animal kingdom.<sup>63</sup> ECM proteins, in particular collagens, play key roles in nervous system development, in cellular maintenance and repair, and in tissue responses to diseases such as injury or neoplasia.<sup>64</sup> Collagens in the PNS provide a scaffold for Schwann cells and support neurite outgrowth.<sup>65,66</sup> A central role for collagen IV in axon guidance and neurite outgrowth is also supported by studies in simple model organisms.<sup>23,24</sup> A missense mutation in COL4A6 is associated with hearing loss.<sup>67</sup> Collagens in the adult nervous system are produced primarily by cells of mesodermal origin, the endothelial cells, and are found, together with other forms of ECM proteins, in the basement membrane of cerebral blood vessels and at the glia limitans.<sup>64</sup> Upon injury, glial cells express and secret collagen and other ECM proteins.<sup>68</sup> While evidence suggests that this process supports neurite outgrowth (see above), in rats, by contributing to the formation of the glial scar, it could also inhibit axonal regeneration.<sup>68</sup> Interestingly although, engineered biopolymer scaffolds containing collagen are explored as a therapeutic support for nerve repair after injury.<sup>69</sup>

Our study shows, for the first time, that one subunit of collagen IV, subunit 6, is a candidate for regulating axonal branching of nigral DA neurons in a mammalian model. Because we had observed large striatal DA differences and large ventral midbrain *Col4a6* expression differences in C56BL/6 versus A/J mice, we then tested if these two mouse strains also differed in striatal axonal branching. We observed less density of TH-positive axons in the dorsal striatum of A/J compared to C57BL/6J mice. We found no difference in TH-positive neuronal profiles in the SN of these two smouse strains. Thus, the lower density of TH-positive axons in the striata of A/J mice most likely reflects a lesser degree of axonal branching of the nigral DA neurons in that strain. To ensure that our strain differences reflect properties of the nigrostriatal circuitry and not all projecting DA neurons of the ventral midbrain, we assessed brain areas that receive projections from the VTA, the basolateral amygdala and piriform cortex. In these areas, we observed no difference of TH-positive axonal branching between C57BL/6J and A/J mice. In mouse strains other than those used here, studies<sup>11,15</sup> reported strain-dependent differences in the number of midbrain populations of DA neurons. Using recombinant inbred intercrosses generated from CC strains, recent studies showed significant effect of genetic background on locomotor behavior<sup>45</sup> and response to cocaine,<sup>44</sup> illustrating how the CC family can serve as

useful model for identifying further QTLs and genetic variants that govern structure and function of DA neurons.

Thus, we identified a locus linked to DA level in the dorsal striatum of mice, and highlighted *Col4a6* as a novel gene candidate whose product may govern axonal branching in that brain region in mammals. Because these are the structures that are affected early in PD,<sup>70</sup> we propose that further measurements of striatal DA in additional CC strains and a better understanding of the actions of collagen IV on DA neurons may open the way for better understanding of the early phases of this disease.

## ACKNOWLEDGMENTS

Lasse Sinkkonen and Manuel Buttini thank the Luxembourg National Research Fund (FNR) for funding support (FNR CORE C15/BM/10406131 grant). Michel Mittelbronn thanks the FNR for funding support (FNR PEARL P16/BM/11192868 grant). Klaus Schughart thanks the support by intra-mural grants from the Helmholtz-Association (Program Infection and Immunity). The authors thank Dr. A. Ginolhac, Dr. D. Coowar, Dr. R. Halder, Z. Hodak and the animal caretakers for their contributions.

## CONFLICT OF INTEREST

The authors declare no conflicts of interest.

## DATA AVAILABILITY STATEMENT

Data sharing is not applicable to this article as no new data were created or analyzed in this study.

## ORCID

Lasse Sinkkonen  <https://orcid.org/0000-0002-4223-3027>  
Manuel Buttini  <https://orcid.org/0000-0003-1805-0279>

## REFERENCES

- Hassan A, Benarroch EE. Heterogeneity of the midbrain dopamine system: implications for Parkinson disease. *Neurology*. 2015;85:1795-1805.
- Vogt Weisenhorn DM, Giesert F, Wurst W. Diversity matters - heterogeneity of dopaminergic neurons in the ventral mesencephalon and its relation to Parkinson's disease. *J Neurochem*. 2016;139(suppl 1):8-26.
- Del Rey NL-G, Quiroga-Varela A, Garbayo E, et al. Advances in Parkinson's disease: 200 years later. *Front Neuroanat*. 2018;12:113.
- Gilgun-Sherki Y, Djaldetti R, Melamed E, Offen D. Polymorphism in candidate genes: implications for the risk and treatment of idiopathic Parkinson's disease. *Pharmacogenomics J*. 2004;4:291-306.
- Jankovic J, McDermott M, Carter J, et al. Variable expression of Parkinson's disease: a base-line analysis of the DATATOP cohort. *Parkinson Study Group Neurol*. 1990;40:1529-1534. <https://doi.org/10.1212/WNL.40.10.1529>
- van Rooden SM, Colas F, Martínez-Martín P, et al. Clinical subtypes of Parkinson's disease. *Mov Disord*. 2011;26:51-58.
- Kalinderi K, Fidani L, Katsarou Z, Bostantjopoulou S. Pharmacological treatment and the prospect of pharmacogenetics in Parkinson's disease. *Int J Clin Pract*. 2011;65:1289-1294.
- Kaplan N, Vituri A, Korczyn AD, et al. Sequence variants in SLC6A3, DRD2, and BDNF genes and time to levodopa-induced dyskinesias in Parkinson's disease. *J Mol Neurosci*. 2014;53:183-188.
- Klafke R, Wurst W, Prakash N. Genetic control of rodent midbrain dopaminergic neuron development in the light of human disease. *Pharmacopsychiatry*. 2008;41(suppl 1):S44-S50.
- Nadeau JH, Auwerx J. The virtuous cycle of human genetics and mouse models in drug discovery. *Nat Rev Drug Discov*. 2019;18:255-272.
- Baker H, Joh TH, Reis DJ. Genetic control of number of midbrain dopaminergic neurons in inbred strains of mice: relationship to size and neuronal density of the striatum. *Proc Natl Acad Sci U S A*. 1980;77:4369-4373.
- Cabib S, Puglisi-Allegra S, Ventura R. The contribution of comparative studies in inbred strains of mice to the understanding of the hyperactive phenotype. *Behav Brain Res*. 2002;130:103-109.
- Vadasz C, Sziraki I, Sasvari M, et al. Analysis of the mesotelencephalic dopamine system by quantitative-trait locus introgression. *Neurochem Res*. 1998;23:1337-1354.
- Vadász C, Sziráki I, Murthy LR, et al. Genetic determination of mesencephalic tyrosine hydroxylase activity in the mouse. *J Neurogenet*. 1987;4:241-252.
- Zaborszky L, Vadász C. The midbrain dopaminergic system: anatomy and genetic variation in dopamine neuron number of inbred mouse strains. *Behav Genet*. 2001;31:47-59.
- Brooks SP, Pask T, Jones L, Dunnett SB. Behavioural profiles of inbred mouse strains used as transgenic backgrounds. I: motor tests. *Genes Brain Behav*. 2004;3:206-215.
- Hamre K, Tharp R, Poon K, Xiong X, Smeley RJ. Differential strain susceptibility following 1-methyl-4-phenyl-1,2,3,6-tetrahydropyridine (MPTP) administration acts in an autosomal dominant fashion: quantitative analysis in seven strains of *Mus musculus*. *Brain Res*. 1999;828:91-103.
- Ingram DK, London ED, Reynolds MA, Waller SB, Goodrick CL. Differential effects of age on motor performance in two mouse strains. *Neurobiol Aging*. 1981;2:221-227.
- de Jong S, Fuller TF, Janson E, et al. Gene expression profiling in C57BL/6J and a/J mouse inbred strains reveals gene networks specific for brain regions independent of genetic background. *BMC Genomics*. 2010;11:20.
- Peters LL, Robledo RF, Bult CJ, Churchill GA, Paigen BJ, Svenson KL. The mouse as a model for human biology: a resource guide for complex trait analysis. *Nat Rev Genet*. 2007;8:58-69.
- Churchill GA, Airey DC, Allayee H, et al. The collaborative cross, a community resource for the genetic analysis of complex traits. *Nat Genet*. 2004;36:1133-1137.
- La Manno G, Gyllborg D, Codeluppi S, et al. Molecular diversity of midbrain development in mouse, human, and stem cells. *Cell*. 2016;167:566-580.e19.
- Mirre C, Le Parco Y, Knibiehler B. Collagen IV is present in the developing CNS during drosophila neurogenesis. *J Neurosci Res*. 1992;31:146-155.
- Takeuchi M, Yamaguchi S, Yonemura S, et al. Type IV collagen controls the Axogenesis of cerebellar granule cells by regulating basement membrane integrity in zebrafish. *PLoS Genet*. 2015;11:e1005587.
- Gui Y, Thomas MH, Garcia P, et al. Pituitary tumor transforming gene 1 orchestrates gene regulatory variation in mouse ventral midbrain during aging. *Front Genet*. 2020;11:566734.
- Karunakaran S, Diwakar L, Saeed U, et al. Activation of apoptosis signal regulating kinase 1 (ASK1) and translocation of death-associated protein, Daxx, in substantia nigra pars compacta in a mouse model of Parkinson's disease: protection by alpha-lipoic acid. *FASEB J*. 2007;21:2226-2236.
- Sarsani VK, Ragupathy N, Fiddes IT, et al. The genome of C57BL/6J "eve", the mother of the laboratory mouse genome reference strain. *G3 (Bethesda)*. 2019;9:1795-1805.

28. Jaeger C, Glaab E, Michelucci A, et al. The mouse brain metabolome: region-specific signatures and response to excitotoxic neuronal injury. *Am J Pathol.* 2015;185:1699-1712.
29. Jäger C, Hiller K, Buttini M. Metabolic profiling and quantification of neurotransmitters in mouse brain by gas chromatography-mass spectrometry. *Curr Protoc Mouse Biol.* 2016;6:333-342.
30. Schindelin J, Arganda-Carreras I, Frise E, et al. Fiji: an open-source platform for biological-image analysis. *Nat Methods.* 2012;9:676-682.
31. Masliah E, Rockenstein E, Veinbergs I, et al. Dopaminergic loss and inclusion body formation in alpha-synuclein mice: implications for neurodegenerative disorders. *Science.* 2000;287:1265-1269.
32. Ashrafi A, Garcia P, Kollmus H, et al. Absence of regulator of G-protein signaling 4 does not protect against dopamine neuron dysfunction and injury in the mouse 6-hydroxydopamine lesion model of Parkinson's disease. *Neurobiol Aging.* 2017;58:30-33.
33. Schöndorf DC, Aureli M, McAllister FE, et al. iPSC-derived neurons from GBA1-associated Parkinson's disease patients show autophagic defects and impaired calcium homeostasis. *Nat Commun.* 2014;5:4028.
34. Reinhardt P, Glatza M, Hemmer K, et al. Derivation and expansion using only small molecules of human neural progenitors for neurodegenerative disease modeling. *PLoS ONE.* 2013;8:e59252.
35. Mulligan MK, Mozhui K, Prins P, Williams RW. GeneNetwork: a toolbox for systems genetics. *Methods Mol Biol.* 2017;1488:75-120.
36. Sittig LJ, Carbonetto P, Engel KA, Krauss KS, Palmer AA. Integration of genome-wide association and extant brain expression QTL identifies candidate genes influencing prepulse inhibition in inbred F1 mice. *Genes Brain Behav.* 2016;15(2):260-270.
37. Gonzales NM, Palmer AA. Fine-mapping QTLs in advanced intercross lines and other outbred populations. *Mamm Genome.* 2014;25:271-292.
38. Gonzales NM, Seo J, Hernandez Cordero AI, et al. Genome wide association analysis in a mouse advanced intercross line. *Nat Commun.* 2018;9:5162.
39. Parker CC, Gopalakrishnan S, Carbonetto P, et al. Genome-wide association study of behavioral, physiological and gene expression traits in outbred CFW mice. *Nat Genet.* 2016;48:919-926.
40. Zhou X, Stephens M. Genome-wide efficient mixed-model analysis for association studies. *Nat Genet.* 2012;44:821-824.
41. Ashbrook DG, Arends D, Prins P, et al. A platform for experimental precision medicine: the extended BXD mouse family. *Cell Syst.* 2021; 12:235-247. e9.s.
42. Belknap JK. Effect of within-strain sample size on QTL detection and mapping using recombinant inbred mouse strains. *Behav Genet.* 1998; 28:29-38.
43. Philip VM, Sokoloff G, Ackert-Bicknell CL, et al. Genetic analysis in the collaborative cross breeding population. *Genome Res.* 2011;21: 1223-1238.
44. Schoenrock SA, Oreper D, Farrington J, et al. Perinatal nutrition interacts with genetic background to alter behavior in a parent-of-origin-dependent manner in adult collaborative cross mice. *Genes Brain Behav.* 2018;17:e12438.
45. Schoenrock SA, Kumar P, Gómez-A A, et al. Characterization of genetically complex collaborative cross mouse strains that model divergent locomotor activating and reinforcing properties of cocaine. *Psychopharmacology (Berl).* 2020;237:979-996.
46. Gepshtein S, Li X, Snider J, Plank M, Lee D, Poizner H. Dopamine function and the efficiency of human movement. *J Cogn Neurosci.* 2014;26:645-657.
47. Lein ES, Hawrylycz MJ, Ao N, et al. Genome-wide atlas of gene expression in the adult mouse brain. *Nature.* 2007;445:168-176.
48. Ma Y, Hof PR, Grant SC, et al. A three-dimensional digital atlas database of the adult C57BL/6J mouse brain by magnetic resonance microscopy. *Neuroscience.* 2005;135:1203-1215.
49. Hegmann JP, Possidente B. Estimating genetic correlations from inbred strains. *Behav Genet.* 1981;11:103-114.
50. Kollmus H, Fuchs H, Lengerer C, et al. A comprehensive and comparative phenotypic analysis of the collaborative founder strains identifies new and known phenotypes. *Mamm Genome.* 2020;31: 30-48.
51. Maurano MT, Humbert R, Rynes E, et al. Systematic localization of common disease-associated variation in regulatory DNA. *Science.* 2012;337:1190-1195.
52. Gelse K, Pöschl E, Aigner T. Collagens-structure, function, and biosynthesis. *Adv Drug Deliv Rev.* 2003;55:1531-1546. <https://doi.org/10.1016/j.addr.2003.08.002>
53. Ricard-Blum S. The collagen family. *Cold Spring Harb Perspect Biol.* 2011;3:a004978.
54. Mao M, Alavi MV, Labelle-Dumais C, Gould DB. Type IV Collagens and Basement Membrane Diseases: Cell Biology and Pathogenic Mechanisms. *Curr Top Membr.* 2015;76:61-116. <https://doi.org/10.1016/bs.ctm.2015.09.002>
55. Carbonetto S, Gruver MM, Turner DC. Nerve fiber growth in culture on fibronectin, collagen, and glycosaminoglycan substrates. *J Neurosci.* 1983;11:2324-2335.
56. Ferri ALM, Cavallaro M, Braida D, et al. Sox2 deficiency causes neurodegeneration and impaired neurogenesis in the adult mouse brain. *Development.* 2004;131:3805-3819.
57. Berezovsky AD, Poisson LM, Cherba D, et al. Sox2 promotes malignancy in glioblastoma by regulating plasticity and astrocytic differentiation. *Neoplasia.* 2014;16:193-206. 206.e19-25.
58. Fang X, Yoon J-G, Li L, et al. The SOX2 response program in glioblastoma multiforme: an integrated ChIP-seq, expression microarray, and microRNA analysis. *BMC Genomics.* 2011;12:11.
59. Surmeier DJ. Determinants of dopaminergic neuron loss in Parkinson's disease. *FEBS J.* 2018;285:3657-3668.
60. Keele GR, Crouse WL, Kelada SNP, Valdar W. Determinants of QTL mapping power in the realized collaborative cross. *G3 (Bethesda).* 2019;9:1707-1727.
61. Chesler EJ. Out of the bottleneck: the diversity outcross and collaborative cross mouse populations in behavioral genetics research. *Mamm Genome.* 2014;25:3-11.
62. Saul MC, Philip VM, Reinholdt LG, Chesler EJ. High-diversity mouse populations for complex traits. *Trends Genet.* 2019;35:501-514.
63. Vecino E, Kwok JCF. The extracellular matrix in the nervous system: the good and the bad aspects. In: Travascio F, ed. *Composition and Function of the Extracellular Matrix in the Human Body.* IntechOpen Limited, London: InTech; 2016.
64. Rutka JT, Apodaca G, Stern R, Rosenblum M. The extracellular matrix of the central and peripheral nervous systems: structure and function. *J Neurosurg.* 1988;69:155-170.
65. Chen P, Cescon M, Bonaldo P. The role of collagens in peripheral nerve myelination and function. *Mol Neurobiol.* 2015;52:216-225.
66. Lein PJ, Higgins D, Turner DC, Flier LA, Terranova VP. The NC1 domain of type IV collagen promotes axonal growth in sympathetic neurons through interaction with the alpha 1 beta 1 integrin. *J Cell Biol.* 1991;113:417-428.
67. Rost S, Bach E, Neuner C, et al. Novel form of X-linked non-syndromic hearing loss with cochlear malformation caused by a mutation in the type IV collagen gene COL4A6. *Eur J Hum Genet.* 2014;22:208-215.
68. Liesi P, Kauppinen T. Induction of type IV collagen and other basement-membrane-associated proteins after spinal cord injury of the adult rat may participate in formation of the glial scar. *Exp Neurol.* 2002;173: 31-45.
69. Li X, Dai J. Bridging the gap with functional collagen scaffolds: tuning endogenous neural stem cells for severe spinal cord injury repair. *Biomater Sci.* 2018;6:265-271.

70. Kordower JH, Olanow CW, Dodiya HB, et al. Disease duration and the integrity of the nigrostriatal system in Parkinson's disease. *Brain*. 2013;136:2419-2431.

#### SUPPORTING INFORMATION

Additional supporting information may be found in the online version of the article at the publisher's website.

**How to cite this article:** Thomas MH, Gui Y, Garcia P, et al. Quantitative trait locus mapping identifies a locus linked to striatal dopamine and points to collagen IV alpha-6 chain as a novel regulator of striatal axonal branching in mice. *Genes, Brain and Behavior*. 2021;e12769. doi:10.1111/gbb.12769